Preprints of the 21st IFAC World Congress (Virtual)
Berlin, Germany, July 12-17, 2020

Discrete-Time State-Dependent Proportional-Integral Control for Torque Tracking of Hydrostatic Transmissions

Dang Ngoc Danh *, **Harald Aschemann** **

* *Chair of Mechatronics, University of Rostock, Rostock D-18059, Germany (e-mail: Ngoc.Dang@uni-rostock.de).*
** *Chair of Mechatronics, University of Rostock, Rostock D-18059, Germany (e-mail: Harald.Aschemann@uni-rostock.de).*

Abstract: This paper presents both design and implementation of a discrete-time proportional-integral (PI) tracking control for the desired output torque of a nonlinear hydrostatic transmission system affected by disturbances and uncertainties. The control is conceived in a decentralized form, in which the bent-axis angle and the torque of the hydraulic motor are controlled separately. The motor bent-axis angle is adjusted by a pure feedforward control law, whereas the torque of the hydraulic motor is controlled using a PI state feedback from a online-solution of the state-dependent Riccati equation. State variables and external disturbances are reconstructed by a discrete-time nonlinear observer. The stability of the closed-loop system as well as the observer are investigated by linear matrix inequalities. The achieved tracking performance indicates the robustness of the overall control structure in the presence of system disturbances and uncertainties. The proposed control is evaluated by means of simulations and experiments using the dedicated test rig at the Chair of Mechatronics, University of Rostock.

Keywords: Decentralized Control, Hydrostatic Transmission, State-Dependent Riccati Equation, Discrete-Time Control, State and Disturbance Observer, Linear Matrix Inequalities

1. INTRODUCTION

Hydrostatic transmissions (HSTs) are widely used in classical industrial applications like heavy working machines, construction and agriculture machinery and off-road vehicles, cf. Schulte (2007). They are recently present also in wind turbines, cf. Schulte (2014), and power-split gearboxes, cf. Shamshirband et al. (2014). HSTs are often preferred in comparison to conventional mechanical gearboxes due to their high power density in combination with a continuously variable transmission ratio. Moreover, they allow for a directional reversion without changing gears as well as wearless braking, see Aschemann (2013). Thanks to a high flexibility regarding the geometrical arrangement, hydrostatic transmissions are employed in numerous drive train designs. Fig. 1 depicts the principle structure of a

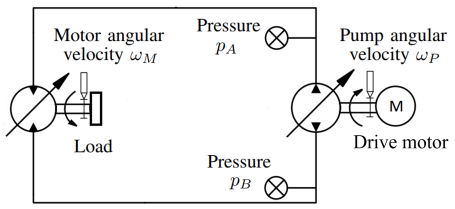

Fig. 1. Principle structure of an HST system.

hydrostatic transmission system. It typically consists of two main components – a hydraulic pump and a hydraulic motor, each with a variable volumetric displacement – that are connected in a closed circuit by means of hydraulic hoses. The pump is driven by an engine or an electric drive, the mechanical power supplied to the system is converted to hydraulic power in form of pressurized fluid flow, and transmitted to the hydraulic motor, where it is converted back to mechanical power at the output shaft.

The axial piston type represents the most popular structure of hydraulic pumps and motors. With this structure, the transmission ratio can be adjusted by changing the swash-plate angle of the hydraulic pump, by altering the axial bent angle of the hydraulic motor or by changing both simultaneously by means of the displacement units. As a result, both torque and angular velocity of the hydraulic motor can be controlled independently according to the purpose of the specific application. For the tracking control of the angular velocity, several concepts have already been proposed, see Dang (2018). Tracking control designs for the motor torque have been published in Aschemann (2017) and Prabel (2017). These control approaches take advantage of extended linearization or Takagi-Sugeno techniques and are designed in the continuous-time domain.

In current industrial practice, gain-scheduled-PID controllers are still the typical choice to control hydrostatic transmissions, see Schulte (2007). As the derivative term may be critical w.r.t. high-frequency noise, PI controllers may be preferable to PID controllers in such cases, cf. Dogruer (2018). Aiming at a digital control implementation, this paper presents the design and implementation of a discrete-time decentralized control structure: a simple

feedforward control is deployed for the bent-axis angle of the hydraulic motor, whereas the motor torque is regulated by the PI state-feedback control based on SDRE techniques. The tracking control performance is investigated by means of both simulation and experiments using a validated model of the dedicated test rig which is available at Chair of Mechatronics, University of Rostock.

Fig. 2. HST test rig at Chair of Mechatronics, University of Rostock.

2. NONLINEAR MODEL OF THE HYDROSTATIC TRANSMISSION

This section presents briefly the model for the HST system, which can be found in more detail in Sun (2015).

2.1 Hydraulic Subsystem

Pump Flow Rate The pump flow rate q_P is determined by a nonlinear function

$$q_P = \frac{V_P(\alpha_P)\omega_P}{2\pi}, \tag{1}$$

with ω_P as the angular velocity of the pump. The nonlinear relationship between the volumetric displacement $V_P(\alpha_P)$ and the tilt angle α_P of the swashplate is defined by

$$V_P(\alpha_P) = N_P\, A_P\, D_P\, \tan(\alpha_{P,\max} \cdot \tilde{\alpha}_P)\,, \tag{2}$$

with the normalized swashplate angle $\tilde{\alpha}_P = \alpha_P/\alpha_{P,\max}$. Here, the geometrical parameters are the effective piston area A_P, the diameter D_P of the piston circle, and the number N_P of pistons present in the pump. With the maximum volumetric displacement $\tilde{V}_P = \frac{N_P A_P D_P}{2\pi}$, the pump flow rate can be stated as

$$q_P = \tilde{V}_P \tan\left(\alpha_{P,\max} \cdot \tilde{\alpha}_P\right) \omega_P. \tag{3}$$

Motor Flow Rate The hydraulic motor is of a bent-axis design. Therefore, the ideal volume flow rate q_M into the hydraulic motor becomes

$$q_M = \frac{V_M(\alpha_M)\omega_M}{2\pi}, \tag{4}$$

where $V_M(\alpha_M)$ represents the nonlinear volumetric displacement of the motor and ω_M the motor angular velocity. Given the geometrical parameters N_M, A_M, and D_M, the volume flow rate can be written as

$$q_M = \tilde{V}_M \sin\left(\alpha_{M,\max} \cdot \tilde{\alpha}_M\right) \omega_M. \tag{5}$$

Here, a normalized bent-axis angle is introduced according to $\tilde{\alpha}_M = \alpha_M/\alpha_{M,\max}$ as well as the maximum volumetric displacement $\tilde{V}_M = \frac{N_M A_M D_M}{2\pi}$, similar to the pump model.

Dynamics of fluid pressure The pressure dynamics involves the dynamics of the high-pressure and the low-pressure sides of the hydrostatic transmission. For practical reasons, the pressure dynamics is reduced to the dynamics of the difference pressure between the high and low pressure sides. Assuming symmetric physical conditions and negligible pressure losses in the hydraulic hoses, the differential equation for the difference pressure results in

$$\begin{aligned}\Delta\dot{p} = \frac{2}{C_H}\Big(&\tilde{V}_P \tan\left(\alpha_{P,\max}.\tilde{\alpha}_P\right)\omega_P \\ &- \tilde{V}_M sin\left(\alpha_{M,\max}.\tilde{\alpha}_M\right)\omega_M\Big) - \frac{q_U}{C_H}\,,\end{aligned} \tag{6}$$

where q_U is a lumped disturbance caused by the individual leakage flows, and C_H denotes the hydraulic capacitance.

Dynamics of Actuators The dynamics of the displacement units of the pump and the motor are represented by first-order lag models

$$\begin{aligned} T_{uP}\dot{\tilde{\alpha}}_P + \tilde{\alpha}_P &= k_P u_P\,, \\ T_{uM}\dot{\tilde{\alpha}}_M + \tilde{\alpha}_M &= k_M u_M\,. \end{aligned} \tag{7}$$

Here, T_{uP} and T_{uM} denote the corresponding time constants, k_P and k_M the proportional gains, and u_P and u_M the analogue input voltages of the servo valves. In the given physical design, the angles are bounded by $\tilde{\alpha}_P \in [-1, 1]$ and $\tilde{\alpha}_M \in [\epsilon_M, 1],\ \epsilon_M > 0$.

2.2 Mechanical Subsystem

The mechanical aspects of the HST system are governed by the equation of motion for the motor

$$J_V\dot{\omega}_M + d_V\omega_M = \tilde{V}_M\Delta p\, \sin(\alpha_{M,\max} \cdot \tilde{\alpha}_M) - \tau_U\,, \tag{8}$$

where d_V is the damping coefficient, and J_V the mass moment of inertia. A lumped disturbance torque τ_U addresses load disturbances and model uncertainty.

2.3 The Nonlinear Model of the Overall System

Combining all the subsystems discussed, the dynamics of the HST system can be stated by four first-order differential equations as follows

$$\begin{bmatrix}\dot{\tilde{\alpha}}_M \\ \dot{\tilde{\alpha}}_P \\ \Delta\dot{p} \\ \dot{\omega}_M\end{bmatrix} = \begin{bmatrix} -\frac{1}{T_{uM}}\tilde{\alpha}_M + \frac{k_P}{T_{uM}}u_M \\ -\frac{1}{T_{uP}}\tilde{\alpha}_P + \frac{k_M}{T_{uP}}u_P \\ \frac{2\tilde{V}_P}{C_H}\tan(\alpha_P)\omega_P - \frac{2\tilde{V}_M}{C_H}\sin(\alpha_M)\omega_M - \frac{q_U}{C_H} \\ -\frac{d_V}{J_V}\omega_M + \frac{\tilde{V}_M}{J_V}\sin(\alpha_M)\Delta p - \frac{\tau_U}{J_V}\end{bmatrix}, \tag{9}$$

where $\alpha_M = \tilde{\alpha}_M \cdot \alpha_{M,\max}$ as well as $\alpha_P = \tilde{\alpha}_P \cdot \alpha_{P,\max}$ have been used and the control inputs are given by u_P and u_M.

3. DISCRETE TIME CONTROL DESIGN

In the decentralized control structure, the motor bent-axis angle and the motor torque are controlled separately.

3.1 Feedforward Control of the Motor Bent-Axis Angle

The dynamics of the motor tilt angle consists only of the first equation in (9), which represents a simple first-order lag behaviour

$$\dot{\tilde{\alpha}}_M = -\frac{1}{T_{uM}}\,\tilde{\alpha}_M + \frac{k_M}{T_{uM}}\,u_M. \tag{10}$$

Accordingly, a feedforward control is sufficient for reference tracking. Applying the explicit Euler method, the discrete-time system representation with the time index k becomes

$$\tilde{\alpha}_M(k+1) = \left(1 - T_s\frac{1}{T_{uM}}\right)\tilde{\alpha}_M(k) + T_s\frac{k_M}{T_{uM}}u_M(k). \tag{11}$$

Here, T_s is the constant time step size. The inverse dynamics of the motor displacement unit becomes

$$u_M = \frac{T_{uM}}{T_s k_M}\tilde{\alpha}_M(k+1) - \left(\frac{T_{uM}}{T_s k_M} - \frac{1}{k_M}\right)\tilde{\alpha}_M(k). \tag{12}$$

The feedforward control law is made causal by shifting the desired value $\tilde{\alpha}_{M,d}$ one time step backward, resulting in

$$u_M = \frac{T_{uM}}{T_s k_M}\tilde{\alpha}_{M,d}(k) - \left(\frac{T_{uM}}{T_s k_M} - \frac{1}{k_M}\right)\tilde{\alpha}_{M,d}(k-1). \tag{13}$$

3.2 State Feedback Tracking Control Design

The relevant state equations for the motor torque control design are given by the second and third equations in (9), which can be written by means of state- and parameter-dependent matrices and vectors as follows

$$\begin{aligned} \dot{\mathbf{x}} &= \mathbf{A}(\tilde{\alpha}_P, \omega_P)\,\mathbf{x} + \mathbf{b}\,u + \mathbf{e}\,v\ , \\ y &= \mathbf{c}^T(\tilde{\alpha}_M)\,\mathbf{x}\,. \end{aligned} \tag{14}$$

In detail, the system (14) description reads

$$\begin{aligned} \begin{bmatrix} \dot{\tilde{\alpha}}_P \\ \Delta\dot{p} \end{bmatrix} &= \begin{bmatrix} -\frac{1}{T_{uP}} & 0 \\ f(\cdot) & 0 \end{bmatrix}\begin{bmatrix} \tilde{\alpha}_P \\ \Delta p \end{bmatrix} + \begin{bmatrix} \frac{k_P}{T_{uP}} \\ 0 \end{bmatrix} u_P + \begin{bmatrix} 0 \\ \frac{1}{C_H} \end{bmatrix} v, \\ y &= \begin{bmatrix} 0 & f_c(\tilde{\alpha}_M) \end{bmatrix}\begin{bmatrix} \tilde{\alpha}_P \\ \Delta p \end{bmatrix}. \end{aligned} \tag{15}$$

Here, $v = -2\tilde{V}_M\omega_M \sin(\alpha_{M,\max}\cdot\tilde{\alpha}_M) - q_U$ defines a lumped disturbance term, and y is the output torque of the hydraulic motor. The state- and parameter-dependent (SPD) nonlinear functions $f(\tilde{\alpha}_P, \omega_P)$ and $f_c(\tilde{\alpha}_M)$ are given by

$$\begin{aligned} f(\tilde{\alpha}_P, \omega_P) &= \frac{2\tilde{V}_P\omega_P \mathrm{sinc}(\alpha_{P,\max}\cdot\tilde{\alpha}_P)\cdot\alpha_{P,\max}}{C_H\cos(\alpha_{P,\max}\cdot\tilde{\alpha}_P)}, \\ f_c(\tilde{\alpha}_M) &= \tilde{V}_M\sin(\alpha_{M,\max}\cdot\tilde{\alpha}_M)\ . \end{aligned} \tag{16}$$

In this design model, the state variable $\tilde{\alpha}_M$ is considered as a scheduling parameter.

The design is based on SDRE techniques, at each time step the SPD system matrix is calculated and employed in the discrete-time linear quadratic regulator (LQR) design to obtain the corresponding feedback gain. The term v in (14) is discarded in this step and is addressed separately. For the PI feedback, the system is extended by an integral term w, which is defined by

$$\dot{w} = e = r - y. \tag{17}$$

Here, e stands for the tracking error, r is the reference value and y represents the controlled output torque. The extended system becomes

$$\begin{aligned} \dot{\mathbf{x}}_w &= \mathbf{A}_w(\tilde{\alpha}_M, \tilde{\alpha}_P, \omega_P)\,\mathbf{x}_w + \mathbf{b}_w\,u_{FB} + \mathbf{d}_w\,r\ , \\ y &= \mathbf{c}_w^T(\tilde{\alpha}_M)\,\mathbf{x}_w\ , \end{aligned} \tag{18}$$

where the feedback control action u_{FB} is introduced. The extended system matrices read

$$\begin{aligned} &\mathbf{A}_w(\tilde{\alpha}_M, \tilde{\alpha}_P, \omega_P) = \begin{bmatrix} \mathbf{A} & \mathbf{0} \\ -\mathbf{c}^T & 0 \end{bmatrix},\ \mathbf{x}_w = \begin{bmatrix} \mathbf{x} \\ w \end{bmatrix}, \\ &\mathbf{b}_w = \begin{bmatrix} \mathbf{b} \\ 0 \end{bmatrix},\ \mathbf{d}_w = \begin{bmatrix} \mathbf{0} \\ 1 \end{bmatrix}, \mathbf{c}_w^T = \begin{bmatrix} \mathbf{c}^T & 0 \end{bmatrix}. \end{aligned} \tag{19}$$

A successful SDRE control design is guaranteed if Kalman's controllability criterion is fulfilled point-wise in the complete operating range

$$\begin{aligned} \mathbf{Q}_C(\cdot) &= \begin{bmatrix} \mathbf{b}_w & \mathbf{A}_w(\cdot)\,\mathbf{b}_w & \mathbf{A}_w^2(\cdot)\,\mathbf{b}_w \end{bmatrix}, \\ &\det(\mathbf{Q}_C(\cdot)) \neq 0. \end{aligned} \tag{20}$$

In the given case, the determinant is unequal to zero with $\omega_P > 0$ and $\tilde{\alpha}_M \in [\epsilon_M, 1]$, $\epsilon_M > 0$. After an explicit Euler discretization, the system part for the control design can be described in a discrete-time form according to

$$\mathbf{x}_w(k+1) = \mathbf{A}_{wd}\mathbf{x}_w(k) + \mathbf{b}_{wd}\,u_{FB}(k)\ , \tag{21}$$

with $\mathbf{A}_{wd} = \mathbf{I} + T_s\,\mathbf{A}_w$, $\mathbf{b}_{wd} = T_s\,\mathbf{b}_w$. Optimal control techniques, especially discrete-time SDRE techniques, are now employed, which results in a state- and parameter-dependent feedback gain vector $\mathbf{k}_w(\tilde{\alpha}_M, \tilde{\alpha}_P, \omega_P)$. The SDRE design involves the minimization of a quadratic cost function

$$J = \sum_{k=1}^{\infty}\left[\mathbf{x}_w^T(k)\,\mathbf{Q}\,\mathbf{x}_w(k) + R\,u_{FB}^2(k)\right]\ , \tag{22}$$

where $\mathbf{Q} > \mathbf{0}$ is a positive definite weighting matrix for the state vector $\mathbf{x}_w$ and $R > 0$ is a positive weight the for the scalar input u_{FB}. The optimal feedback gain can be determined as the symmetric, positive definite solution $\mathbf{P} = \mathbf{P}^T > 0$ of the discrete-time algebraic Riccati equation

$$\mathbf{A}_{wd}^T[(\mathbf{P} - \mathbf{P}\,\mathbf{b}_{wd}(R + \mathbf{b}_{wd}^T\mathbf{P}\mathbf{b}_{wd})^{-1}\mathbf{b}_{wd}^T\mathbf{P}]\mathbf{A}_{wd} + \mathbf{Q} = \mathbf{P}, \tag{23}$$

leading to the state- and parameter-dependent feedback gain vector

$$\mathbf{k}_w = (R + \mathbf{b}_{wd}^T\mathbf{P}\mathbf{b}_{wd})^{-1}\mathbf{b}_{wd}^T\,\mathbf{P}. \tag{24}$$

Finally, the nonlinear state feedback law results in

$$u_{FB}(k) = -\mathbf{k}_w(\tilde{\alpha}_M, \tilde{\alpha}_P, \omega_P)\,\mathbf{x}_w(k)\ , \tag{25}$$

The implementation of the gain-scheduled control concept is illustrated in Fig. (3). Here, $\mathbf{k}_w^T = \begin{bmatrix} \mathbf{k}^T & k_I \end{bmatrix}$ consists of two components: the component $\mathbf{k^T}$ corresponds to the feedback of the original system state vector $\mathbf{x}$, whereas the component k_I corresponds to a feedback of the integrated tracking error w. Using a polytopic framework, closed-loop stability of the corresponding system matrix $\mathbf{A}_c = \mathbf{A}_{wd} - \mathbf{b}_{wd}\,\mathbf{k}_w^T$ is guaranteed by the existence of a joint Lyapunov function for all four vertices $\mathbf{A}_{c,i}, i = 1, ..., 4$ that result from the maximum and minimum values of the

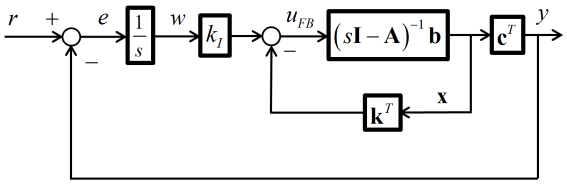

Fig. 3. Implementation of feedback control (presented in continuous form).

nonlinear functions present in the system matrix $\mathbf{A}_c$, see Tanaka (2001) for details. The joint Lyapunov function has been found by means of YALMIP and SeDuMi, see Löfberg (2004); Sturm (1999), satisfying the following set of inequalities

$$\mathbf{P}_0 > 0,\ \mathbf{A}_{c,i}^T\,\mathbf{P}_0\,\mathbf{A}_{c,i} - \mathbf{P}_0 < 0,\quad i \in \{1,...,4\}\ . \tag{26}$$

Moreover, Fig. 4 shows the closed-loop eigenvalue locations of $\mathbf{A}_c$ in the whole working range of the state variables and scheduling variables.

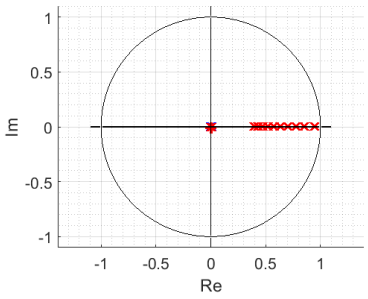

Fig. 4. Eigenvalue locations of the state-dependent closed-loop system matrix.

Disturbance Compensation For a further improvement of tracking performance, the lumped disturbance v defined in (14) needs to be compensated. The z-transfer function from the term $V(z)$ to the controlled output $Y(z)$ becomes

$$G_e(z) = \frac{Y\,(z)}{V\,(z)} = \mathbf{c}^T\,(z\mathbf{I} - \mathbf{A}_c)^{-1}\,\mathbf{e}_d\,. \tag{27}$$

Here, $\mathbf{A}_c = \mathbf{A}_d - \mathbf{b}_d\mathbf{k}^T$ holds with $\mathbf{A}_d = \mathbf{I} + T_s\,\mathbf{A}$, $\mathbf{b}_d = T_s\,\mathbf{b}$ and $\mathbf{e}_d = T_s\,\mathbf{e}$. For an ideal disturbance compensation, the following condition has to be fulfilled by a proper choice of the disturbance compensation law $U_{DC}(z)$

$$Y(z) = G_b(z)\cdot U_{DC}(z) + G_e(z)\cdot V(z) \stackrel{!}{=} 0\ , \tag{28}$$

with $G_b(z) = \mathbf{c}^T\,(z\mathbf{I} - \mathbf{A}_c)^{-1}\,\mathbf{b}_d$. By solving for $U_{DC}(z)$, the dynamic disturbance compensation results in

$$U_{DC}(z) = -\frac{G_e(z)}{G_b(z)}\cdot V(z)\ . \tag{29}$$

In the given case, no zeros are present in the discrete-time system model, hence the minimum-phase system $G_b(z)$ can be inverted, and the compensation law is implementable. With the introduction of a polynomial ansatz for $V(z)$

$$V(z) = k_{V0} + k_{V1}\cdot z, \tag{30}$$

the coefficients k_{V0} and k_{V1} are chosen in such a way that at least the first two coefficients of the numerator polynomial in the transfer function (29) vanish. Using the estimate $\hat{q}_U$, the term v can be evaluated according to (15) and the compensation law becomes

$$u_{DC}(k) = k_{V1}(\tilde{\alpha}_P, \omega_P)v(k) + k_{V0}(\tilde{\alpha}_P, \omega_P)v(k-1). \tag{31}$$

The overall control law for the motor torque, see Fig. 6, is given by the sum of the input signals from feedback control and disturbance compensation

$$u_P = u_{FB} + u_{DC}\ . \tag{32}$$

3.3 Design of a Nonlinear Discrete-Time Observer

The proposed nonlinear control law involves state feedback. With the given sensor equipment at the dedicated test rig, however, some variables are not accessible by measurements. Therefore, a nonlinear observer is designed to reconstruct all the required variables. For this purpose, the state vector $\mathbf{x}_1 = [\,\tilde{\alpha}_P\ \tilde{\alpha}_M\ \Delta p\ \omega_M\,]^T$ in system (9) is extended by integrator-type disturbance models: $\dot{\tau}_U = 0$ for the disturbance torque and, similarly, $\dot{q}_U = 0$ for the leakage volume flow. The extended state vector now reads

$$\mathbf{x}_e = [\,\tilde{\alpha}_P\ \tilde{\alpha}_M\ \Delta p\ \omega_M\ q_U\ \tau_U\,]^T, \tag{33}$$

with the measured outputs

$$\mathbf{y}_m = \begin{bmatrix}\Delta p\\ \omega_M\end{bmatrix} = \begin{bmatrix}0&0&1&0&0&0\\0&0&0&1&0&0\end{bmatrix}\mathbf{x}_e = \mathbf{C}_m\mathbf{x}_e. \tag{34}$$

The observer is designed based on SDRE techniques by deploying the duality principle in a similar way as in the SDRE feedback control design presented before. The extended system is rewritten using SPD matrices as follows

$$\dot{\mathbf{x}}_e = \mathbf{A}_e\,(\mathbf{x}_1)\,\mathbf{x}_e + \mathbf{B}_e\mathbf{u}, \tag{35}$$

where the SPD system matrix $\mathbf{A}_e\,(\mathbf{x}_1)$ and the extended input matrix $\mathbf{B}_e$ become

$$\mathbf{A}_e = \begin{bmatrix} -\frac{1}{T_{uP}} & 0 & 0 & 0 & 0 & 0\\ 0 & -\frac{1}{T_{uM}} & 0 & 0 & 0 & 0\\ f_1\,(\cdot) & f_2\,(\cdot) & 0 & 0 & -\frac{1}{C_H} & 0\\ 0 & 0 & f_3\,(\cdot) & -\frac{d_V}{J_V} & 0 & -\frac{1}{J_V}\\ 0 & 0 & 0 & 0 & 0 & 0\\ 0 & 0 & 0 & 0 & 0 & 0 \end{bmatrix}$$
$$\mathbf{B}_e^T = \begin{bmatrix} \frac{k_P}{T_{uP}} & 0 & 0&0&0&0\\ 0 & \frac{k_M}{T_{uM}} & 0&0&0&0 \end{bmatrix} \tag{36}$$

Given the available measurements, this selection for SPD system matrix satisfies Kalman's observability criterion, which represents the precondition for a successful SDRE observer design. The state- and parameter-dependent functions in the extended system matrix read

$$f_1\,(\tilde{\alpha}_P, \omega_P) = \frac{2\tilde{V}_P\omega_P \mathrm{sinc}\,(\alpha_{P,\max}\cdot\tilde{\alpha}_P)\,\alpha_{P,max}}{C_H\cos\,(\alpha_{P,\max}\cdot\tilde{\alpha}_P)},$$
$$f_2\,(\tilde{\alpha}_M, \omega_M) = \frac{-2\tilde{V}_M\omega_M \mathrm{sinc}\,(\alpha_{M,\max}\cdot\tilde{\alpha}_M)\,\alpha_{M,max}}{C_H}, \tag{37}$$
$$f_3\,(\tilde{\alpha}_M) = \frac{\tilde{V}_M\sin\,(\alpha_{M,\max}\cdot\tilde{\alpha}_M)}{J_V}\ .$$

Again, the design model is time-discretized using the explicit Euler method, resulting in

$$\mathbf{x}_e\,(k+1) = \mathbf{A}_{ed}\;\mathbf{x}_e\,(k) + T_s\mathbf{B}_e\mathbf{u}\,(k)\,, \tag{38}$$

with $\mathbf{A}_{ed} = \mathbf{I} + T_s\mathbf{A}_e$ and $\mathbf{B}_{ed} = T_s\mathbf{B}_e$. Finally, the state and disturbance observer is given by

$$\hat{\mathbf{x}}_e\,(k+1) = \mathbf{A}_{ed}\hat{\mathbf{x}}_e\,(k) + \mathbf{B}_e\mathbf{u}\,(k) + \mathbf{H}\,(\mathbf{y}_m - \mathbf{C}_m\hat{\mathbf{x}}_e\,(k))\,. \tag{39}$$

Here, the observer gain matrix $\mathbf{H}$ is determined by discrete-time SDRE techniques. The cost function involves quadratic terms for the observer error $\tilde{\mathbf{x}}_\mathbf{e} = \mathbf{x}_\mathbf{e} - \hat{\mathbf{x}}_\mathbf{e}$ and the measurement vector $\boldsymbol{\upsilon}_e$ according to

$$J_e = \sum_{k=1}^{\infty}\left[\tilde{\mathbf{x}}_e^T\,(k)\,\mathbf{Q}_e\tilde{\mathbf{x}}_e\,(k) + \boldsymbol{\upsilon}_e^T\,(k)\,\mathbf{R}_e\boldsymbol{\upsilon}_e\,(k)\right]\,, \tag{40}$$

where the weighting matrices $\mathbf{Q}_e > 0$ and $\mathbf{R}_e > 0$ are symmetric positive definite diagonal matrices. The optimal observer gain matrix can be determined in the form of online solutions $\mathbf{P}_e = \mathbf{P}_e^T > 0$ of a discrete-time algebraic Riccati equation

$$\mathbf{A}_{ed}^T\left[(\mathbf{P}_e - \mathbf{P}_e\,\mathbf{C}_m(\mathbf{R}_e + \mathbf{C}_m^T\mathbf{P}_e\mathbf{C}_m)^{-1}\mathbf{C}_m^T\mathbf{P}_e\right]\mathbf{A}_{ed} + \mathbf{Q}_e = \mathbf{P}_e. \tag{41}$$

The state-dependent observer gain matrix $\mathbf{H}$ becomes

$$\mathbf{H} = (\mathbf{R}_e + \mathbf{C}_m^T\mathbf{P}_e\mathbf{C}_m)^{-1}\mathbf{C}_m^T\mathbf{P}_e. \tag{42}$$

Again, the stability of observer dynamics is investigated using a polytopic framework. Here, a joint Lyapunov function can be determined via LMIs for all $2^3 = 8$ vertex models – corresponding to the minimum and maximum values of functions f_1, f_2 and f_3. Additionally, Fig. 5 illustrates the eigenvalue locations of the state- and parameter-dependent observer error dynamics for the complete range of the state variables as well as scheduling variables.

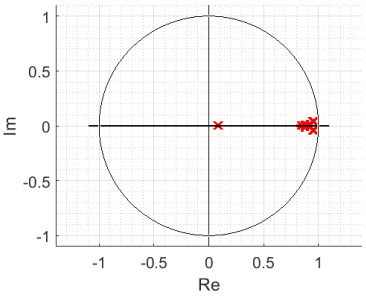

Fig. 5. Eigenvalue locations of the observer error dynamics.

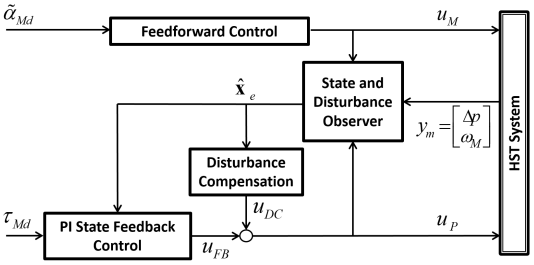

Fig. 6. Block diagram of the implemented control structure.

4. IMPLEMENTATION RESULTS

4.1 Simulation Results

The simulations are performed using the nonlinear system model of the hydrostatic transmission derived in Sect. 2. Here, a simulation step size of 0.05 sec is employed. To obtain realistic and reliable results, measurement noise is added to the output signals and the disturbance torque and leakage volume flow are considered by the following models:

$$\begin{aligned} q_U &= 1\cdot 10^{-12}\Delta p\,, \\ \tau_U &= 0.1 J_V\dot{\omega}_M + 7\tanh\left(\frac{\omega_M}{0.1}\right)\,. \end{aligned} \tag{43}$$

The desired motor torque τ_{Md} and the desired motor tilt angle $\tilde{\alpha}_{Md}$ are used as reference trajectories, see Figs. 7 and 8. The angular velocity of the pump ω_P, which represents a scheduling variable, is depicted in Fig. 9. As saturating inputs are not taken into account in this study, these trajectories are designed properly to avoid any saturation of the displacement units due to the limits of mechanical design. The estimation quality of the dimensionless pump

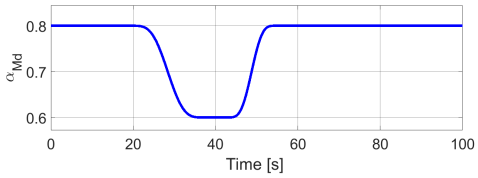

Fig. 7. Desired trajectory for the motor bent-axis angle.

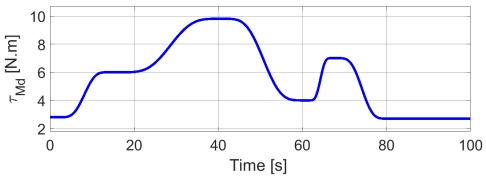

Fig. 8. Desired trajectory for hydraulic torque.

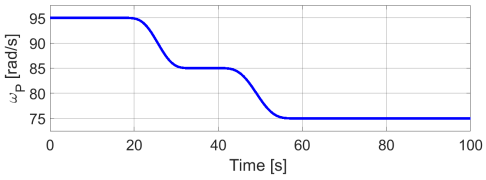

Fig. 9. Variations of hydraulic pump angular velocity.

swashplate angle $\tilde{\alpha}_P$, which is not measurable at the test rig, is illustrated in Fig. 10 whereas the simulated and estimates values for the unknown leakage flow q_U are shown in Fig. 11. The results show a quite good matching of the estimated and the simulated values that indicates a high performance of the proposed nonlinear observer.

Fig. 12 shows the comparison of simulated and estimated values of the motor bent-axis angle. The result shows clearly that a good trajectory tracking is achieved by feedforward control alone.

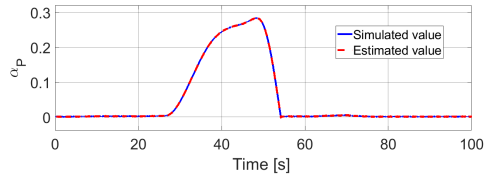

Fig. 10. Simulated and estimated values for $\tilde{\alpha}_P$.

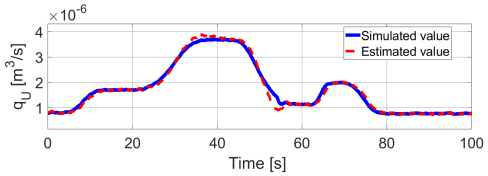

Fig. 11. Simulated and estimated values for q_U.

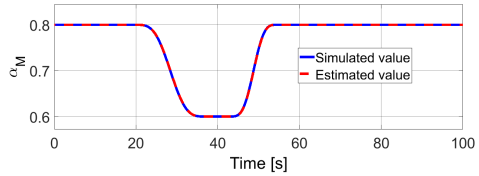

Fig. 12. Simulated and estimated values for $\tilde{\alpha}_M$.

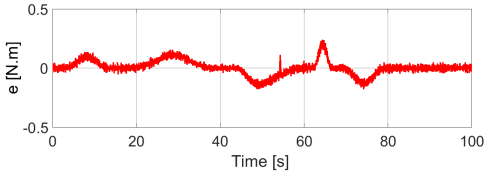

Fig. 13. Tracking error of the hydraulic torque τ_M.

4.2 Experiments

After successful results from simulation studies, the discrete-time control structure has been implemented on the dedicated test rig using an identical sampling time of $T_s = 0.05$ sec. An experimental result for the tracking error is shown in Fig. 14. Obviously, a little higher noise level is present caused by effects at the real equipment. The achieved accuracy, however, indicates an equivalent performance for motor torque tracking as in the simulation and validates the proposed control approach.

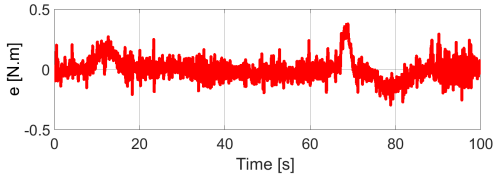

Fig. 14. Tracking errors for the motor torque control at the test rig.

5. CONCLUSIONS

In this paper, a discrete-time tracking control of desired trajectories for the motor torque of a hydrostatic transmission has been investigated. Based on a decentralized structure, a simple discrete feedforward control is designed for the displacement unit of the motor, which allows for a sufficiently accurate tracking of desired trajectories for the motor bent-axis angle. For the tracking of the motor torque, a PI state feedback control as well as an observer have been designed and implemented using a real-time solution of the state-dependent Riccati equation. Here, robust stability has been shown by LMI techniques. Simulation and experimental results indicate the high accuracy and performance of the implemented nonlinear control structure that counteracts efficiently both model uncertainty and external disturbances.

REFERENCES

Schulte, H. (2007). Control-Oriented Modeling of Hydrostatic Transmission Using Takagi-Sugeno Fuzzy Systems. In *Proc. of IEEE Intern. Fuzzy Systems Conference*, 1–6, London, UK.

Shamshirband, S., Petkovic, D., Amini, A., Anuar, N., Nikolic, V., Cojbaic, Z., Kiah, M., and Gani, A. (2014). Support Vector Regression Methodology for Wind Turbine Reaction Torque Prediction With Power-Split Hydrostatic Continuous Variable Transmission. *Energy*, 67:623–630.

Aschemann, H. and Sun, H. (2013): Decentralised Flatness-Based Control of a Hydrostatic Drive Train Subject to Actuator Uncertainty and Disturbances. In *Proc. of Conf. on Methods and Models in Automation and Robotics (MMAR)*, 759–764. Miedzyzdroje, Poland.

Sun, H. (2015): Decentralized Nonlinear Control for a Hydrostatic Drive Train with Unknown Disturbances. *PhD thesis*, University of Rostock, Shaker.

Schulte, H. (2014). Control-Oriented Description of Large Scale Wind Turbines with Hydrostatic Transmission Using Takagi-Sugeno Models. In *Proc. of Conf. on Control Applications (CCA)*, 664–668, Antibes, France.

Dogruer, T. and Tano, N. (2018): Design of PI Controller using Optimization Method in Fractional Order Control Systems. In *Proc. of 3rd IFAC Conference on Advances in Proportional-Integral-Derivative Control*, 52:841–846, Ghent, Belgium.

Aschemann, H. and Prabel, R. (2017): Optimal State feedback Design with Takagi-Sugeno Techniques for the Torque control of a Nonlinear Hydrostatic Transmission. In *Proc. of European Nonlinear Oscillations Conf. (ENOC)*, Budapest, Hungary.

Dang, N. D. and Aschemann, H. (2018): Comparison of Estimator-Based Compensation Schemes for Hydrostatic Transmissions with Uncertainties. In *Proc. of Conf. on Methods and Models in Automation and Robotics (MMAR)*, 692–697, Miedzyzdroje, Poland.

Prabel, R. and Aschemann, H. (2017): Torque Control of a Hydrostatic Transmission Using Extended Linearisation Techniques. In *Proc. of Scandinavian Intern. Conf. on Fluid Power (SICFP)*, Linköping, Sweden.

Tanaka, K. and Wang H. O. (2001): Fuzzy Control Systems Design and Analysis: A Linear Matrix Inequality Approach. *John Wiley and Sons, Inc.*

Sturm, J.F. Using SeDuMi 1.02, A Matlab Toolbox for Optimization Over Symmetric Cones. In *Optimization Methods and Software*, 11-12:625–653.

Löfberg, J. YALMIP: A Toolbox for Modelling and Optimization in MATLAB. In *Proc. of Intern. Symp. on Computer Aided Control Systems Design (CACSD)*, 284–289, LA, USA.